

Probing the Evolution of the Dark Energy Density with Future Supernova Surveys

Yun Wang, Veselin Kostov

Department of Physics & Astronomy, University of Oklahoma, Norman, OK 73019

Katherine Freese

*Michigan Center for Theoretical Physics, Physics Department, University of Michigan,
Ann Arbor, MI 48109*

Joshua A. Frieman

*NASA/Fermilab Astrophysics Center
Fermi National Accelerator Laboratory
Batavia, IL 60510*

and

*Department of Astronomy and Astrophysics and
Center for Cosmological Physics
The University of Chicago
5640 South Ellis Avenue, Chicago, IL 60637*

Paolo Gondolo

*Department of Physics, University of Utah, 115 South 1400 East, Suite 201, Salt Lake City, UT
84112-0830*

(February 2, 2004)

Abstract

The time dependence of the dark energy density can be an important clue to the nature of dark energy in the universe. We show that future supernova data from dedicated telescopes (such as SNAP), when combined with data of nearby supernovae, can be used to determine how the dark energy density $\rho_X(z)$ depends on redshift, if $\rho_X(z)$ is not too close to a constant. For quantitative comparison, we have done an extensive study of a number of dark energy models. Based on these models we have simulated data sets in order to show that we can indeed reconstruct the correct sign of the time dependence of the dark energy density, outside of a degeneracy region centered on $1 + w_0 = -w_1 z_{max}/3$ (where z_{max} is the maximum redshift of the survey, e.g., $z_{max} = 1.7$ for SNAP). We emphasize that, given the same data, one can

obtain much more information about the dark energy density directly (and its time dependence) than about its equation of state.

PACS numbers: 98.80.-k; 98.80.Es; 97.60.Bw

I. INTRODUCTION

Most of the energy in our universe is of unknown nature to us. The amount of this dark energy has been determined by recent experiments, including the Wilkinson Microwave Anisotropy Probe (WMAP) satellite observations [1] of the anisotropy in the cosmic microwave background radiation. Our universe is spatially flat (the three-dimensional equivalent of a two-dimensional plane), with roughly 27% matter and 73% dark energy. Determining the nature of this dark energy is one of the major fundamental challenges in astronomy and physics today.

There are many plausible candidates for dark energy. For example, (1) a cosmological constant, i.e., constant vacuum energy originally proposed by Einstein in his equations of general relativity, (2) a time dependent vacuum energy, or scalar field known as “quintessence”, that evolves dynamically with time [2], or (3) modified Friedmann equation, e.g. the Cardassian models [3–5], that could result as a consequence of our observable universe living as a 3-dimensional brane in a higher dimensional universe. Other proposed modifications to the Friedmann equation include [6]. The time-dependence of the density of dark energy can reveal the nature of dark energy at a fundamental level.

A powerful probe of dark energy is type Ia supernovae (SNe Ia), which can be used as cosmological standard candles to measure how distance depends on redshift in our universe. Observations of SNe Ia have revealed the existence of dark energy in the universe [7,8]. Current SN Ia data are not yet very constraining on the nature of the dark energy [24].

The distance-redshift relation of observed supernovae depends on the nature of dark energy. Most researchers have chosen to parametrize dark energy by its equation of state parameter. However, it has been shown [9,10] that it is extremely difficult to constrain the time-dependence of the dark energy equation of state using supernova searches (or any other technique relying on the luminosity distance); hence one might worry that one cannot differentiate between different dark energy models. Fortunately, it has been shown that one can do much better if one parametrizes the dark energy by its density directly, instead of its equation of state [11–14]. The dark energy density is a more fundamental parameter than the dark energy equation of state parameter. Obtaining the equation of state parameter requires one to perform an additional integral (compared to obtaining the dark energy density); this integral smears out much of the information one could otherwise learn. Hence, given the same data, the uncertainties of the constraints on the dark energy density should be *smaller* than that of the constraints on the dark energy equation of state.

In this paper we focus on extracting information about the dark energy density directly. We will show how well, using future supernova data, one can determine whether the dark energy density changes with time, and whether it increases or decreases with time.

We begin in Section II with the basic equations for using supernovae to study dark energy. In Section III we present four theoretical models which we will study to see how well we can reconstruct the time dependence of the dark energy: Models 1, 2, and 3 have dark energy density that is constant, increasing, and decreasing in time respectively. As our fourth set of models we consider those parametrized by an equation of state $w_X(z) = w_0 + w_1 z$. In Section IV, we simulated SNIa data for these models. In Section V, we use the adaptive iteration method to see how well we can reconstruct the time dependence of the dark energy density for these models: we use three test functions with different time dependences to see

which one best matches the data. For each model we then run 1000 Monte Carlo samples to obtain error bars for our fit. The results are presented in Section VI, followed by the conclusions.

II. BASIC EQUATIONS

Type Ia supernovae (SNe Ia) are our best candidates for cosmological standard candles, because they can be calibrated to have small scatters in their peak luminosity [15,16]. The distance modulus for a standard candle at redshift z is

$$\mu_p(z) \equiv m - M = 5 \log \left(\frac{d_L(z)}{\text{Mpc}} \right) + 25, \quad (1)$$

where m and M are the apparent and absolute magnitudes of the standard candle, and $d_L(z)$ is its luminosity distance.

In a flat Friedmann-Robertson-Walker universe (which we assume in this paper since it is strongly suggested by current CMB data [17,1]) the luminosity distance $d_L(z)$ is given by [18]

$$d_L(z) = \frac{(1+z)c}{H_0} \int_0^z \frac{dz'}{E(z')}, \quad (2)$$

where H_0 is the present value of the Hubble constant, and

$$E(z) \equiv \sqrt{\Omega_m(1+z)^3 + \Omega_X f_X(z)}. \quad (3)$$

Here Ω_m is the present value of the matter density in unit of the critical density $\rho_{\text{crit}} = 3H_0^2/(8\pi G)$, and Ω_X is the present value of the dark energy density in the same units.

The condition for a flat universe imposes the relation

$$\Omega_m + \Omega_X = 1. \quad (4)$$

The dark energy density function

$$f_X(z) = \frac{\rho_X(z)}{\rho_X(0)} \quad (5)$$

describes the redshift dependence of the dark energy density $\rho_X(z)$.

We note that Cardassian models [3–5] contain matter and radiation only (no vacuum), so that in those models, Ω_m and Ω_X are used to refer to *effective* observed matter density and dark energy density respectively.

For a given cosmological model with dark energy density $\rho_X(z)$, or dark energy function $f_X(z)$, we can compare the measured distance modulus of SNe Ia at various redshifts with the predicted distance modulus of a standard candle at these redshifts. A systematic comparison spanning all plausible models yields constraints on the dark energy density $\rho_X(z)$.

III. DARK ENERGY DENSITY FUNCTIONS

In this paper, we are interested in finding what information future SN Ia data can give us about the redshift dependence of the dark energy density. For this purpose, we consider four classes of dark energy densities: (1) constant with redshift, (2) increasing with redshift, (3) decreasing with redshift, and (4) a grid of models which includes some that are non-monotonic with respect to redshift. For each of these four classes we choose simple representative models. Some of the models we choose can be parametrized by a simple equation of state,

$$w_X(z) = w_0 + w_1 z \quad (6)$$

in order to allow simple comparison with previous work in the literature. The simple parametrization of Eq.(6) also allows us to estimate how small a deviation from a constant dark energy density can be determined by our technique. The dark energy density is constant only for $w_0 = -1$ and $w_1 = 0$; any other values of w_0 or of w_1 parametrize deviations from a constant. However, we stress that it is the dark energy density itself, $\rho_X(z)$, that we extract from simulated data, as it is the more fundamental and more easily extracted quantity.

Four Models

The four sample theoretical models we consider are (see Table 1):

Table 1
Dark Energy Models

Model	model parameters	$\rho'_X(z)$
Model 1: Λ CDM	$\Omega_m = 0.3, \Omega_\Lambda = 0.7$	$\rho'_X(z) = 0$
Model 2: quintessence model	$\Omega_m = 0.3, w_q(z) = -1 + 0.5z$	$\rho'_X(z) \geq 0$
Model 3: MP Cardassian model	$\Omega_m^{obs} = 0.3, n = 0.2, q = 2$	$\rho'_X(z) \leq 0$
Model 4: grid of models	$w_X(z) = w_0 + w_1 z$ with arbitrary w_0, w_1	all $\rho'_X(z)$

(1) MODEL 1: For a constant dark energy density, $\rho'_X(z) = 0$, we have a cosmological constant model ($w_0 = -1$ and $w_1 = 0$).

(2) MODEL 2: For an increasing dark energy density, $\rho'_X(z) \geq 0$, we choose a quintessence model with equation of state $w_X(z) = -1 + 0.5z$. Popular quintessence models in which the quintessence field tracks the matter field have $\rho'_X(z) \geq 0$ [10].

(3) MODEL 3: For a decreasing dark energy density, $\rho'_X(z) \leq 0$, we choose a Modified Polytrropic (MP) Cardassian model [4] with $n = 0.2$ and $q = 2$,

$$\rho_X(z) = \rho_{\text{crit}} \Omega_m (1+z)^3 \left\{ \left[1 + \frac{\Omega_m^{-q} - 1}{(1+z)^{3q(1-n)}} \right]^{\frac{1}{q}} - 1 \right\}. \quad (7)$$

MP Cardassian models can have either $\rho'_X(z) \geq 0$ or $\rho'_X(z) \leq 0$. Our previous paper [5] shows the regions of parameter space that fall into the two regimes. We also discussed there that MP Cardassian models can be found with $w_X = p_X/\rho_X < -1$ but with $w = p/\rho \geq -1$, so that the dominant energy condition holds (here, w refers to the total energy density

whereas w_X refers only to the new component in the Friedmann equation that mimics a dark energy). An effective $w_X < -1$ is consistent with recent CMB and large scale structure data [19,20].

(4) MODEL 4: We consider a grid of models of the form Eq.(6), for $-1.2 \leq w_0 \leq -0.5$, and $-1.5 \leq w_1 \leq 0.5$, and a grid spacing of $\Delta w_0 = 0.1$ (0.2 for $w_0 \leq -1$) and $\Delta w_1 = 0.1$. This represents a total of 147 models. This grid includes models with $\rho'_X(z)$ that is monotonically increasing or decreasing with redshift, as well as models with dark energy density that is non-monotonic with redshift. In a moment we will show which values of w_0 and w_1 correspond to a non-monotonic dark energy density.

Although models of the form of Eq.(6) do not correspond exactly to physically motivated models, it is interesting to note that they can approximate a wide range of models. For example, Model 3 (MP Cardassian model with $n = 0.2$, $q = 2$, and $\Omega_m = 0.3$) can be roughly approximated by a dark energy model with $w_X(z) = -1.10 - 0.35z$. The approximate equivalence of these models does not extend to the behavior of dark energy fluctuations but is limited to the average properties of the energy density.

The dark energy density corresponding to Eq.(6) is [11]

$$\rho_X(z) = \rho_X(0)e^{3w_1z} (1+z)^{3(1+w_0-w_1)}. \quad (8)$$

Its derivative with respect to redshift follows as

$$\rho'_X(z) = \rho_X(z) \frac{3(1+w_0+w_1z)}{1+z}. \quad (9)$$

Thus $\rho'_X(z)$ has the same sign as $1+w_0+w_1z$.

Nonmonotonic models: Since z must be positive, models with (i) $w_0 < -1$ and $w_1 > 0$, and models with (ii) $w_0 > -1$ and $w_1 < 0$ have non-monotonic dark energy density $\rho_X(z)$. Models of type (i) have $\rho'(z) < 0$ for $z < z_{crit}$ and $\rho'(z) > 0$ for $z > z_{crit}$ where

$$z_{crit} = |(1+w_0)/w_1|. \quad (10)$$

Models of type (ii) have $\rho'(z) > 0$ for $z < z_{crit}$ and $\rho'(z) < 0$ for $z > z_{crit}$.

All models other than types (i) and (ii) above have monotonic dark energy densities, decreasing with redshift for $w_0 < -1$ and $w_1 < 0$ and increasing with redshift for $w_0 > -1$ and $w_1 > 0$.

IV. SIMULATED DATA

We now construct simulated SN Ia data for dark energy Models 1, 2, 3, and 4 defined above, and investigate if we can recover the original theory from the simulated data.

We simulate the data by distributing SNe Ia in z randomly per 0.1 redshift interval, with the total number per redshift interval as expected for SNAP. Here we assume that SNAP will obtain all SNe Ia in its survey fields up to $z = 1.7$ [25], similar to a supernova pencil beam survey [22,12]. We increase the number of SNe Ia at low redshifts, such that there are a minimum of 50 SNe Ia per 0.1 redshift interval at $z \leq 0.5$. We assume that these

additional low redshift supernovae will come from surveys of nearby SNe Ia. Thus each simulated data set consists of 2300 SNe Ia.

The measured distance modulus for the l -th SN Ia is

$$\mu_0^{(l)} = \mu_p^{(l)} + \epsilon^{(l)} \quad (11)$$

where $\mu_p^{(l)} = \mu_p(z_l)$ is the theoretical prediction in our dark energy model for a SN Ia at redshift z_l [see Eq.(1)], and $\epsilon^{(l)}$ is the uncertainty in the measurement, including observational errors and intrinsic scatters in the SN Ia absolute magnitudes. In the simulated data set, we draw the dispersion $\epsilon^{(l)}$ for the l -th SN Ia from a Gaussian distribution with variance $\Delta m_{int} = 0.16$ mag. We simulate one set of data for each of the four models described in the Table.

V. ESTIMATION OF DARK ENERGY FUNCTIONS

We recover the dark energy function from each simulated data set. A number of techniques may be used to achieve this reconstruction. In this paper we use the adaptive iteration method ¹ introduced by Wang & Garnavich (2001) [11] and Wang & Lovelace (2001) [12] and described briefly here. Our current study builds on our previous work [5]. There we proposed a technique for determining the correct sign of $\rho'_X(z)$ if $\rho_X(z)$ is not too close to a constant. To quantify how close to a constant we can go, in this paper we perform Monte Carlo simulations in order to obtain error bars for our results.

A. Adaptive Iteration Method

We start from the simulated data sets constructed from each of the four models described above. Given our data set, we now proceed as though we did not know which model it came from. We pretend we know nothing about the form of $\rho_X(z)$. In attempting to reconstruct the dark energy density, we run through a series of test functions: we allow the test function $\rho_X^{\text{test}}(z)$ to be an arbitrary function. To approximate the function, we parametrize it by its value at $N + 1$ equally spaced redshift values z_i ($i = 0, 1, 2, \dots, N$, $z_0 = 0$, $z_N = z_{max}$). The values of $\rho_X^{\text{test}}(z)$ at other redshifts are given by linear interpolation, i.e.,

$$\rho_X^{\text{test}}(z) = \left(\frac{z_i - z}{z_i - z_{i-1}} \right) \rho_{i-1} + \left(\frac{z - z_{i-1}}{z_i - z_{i-1}} \right) \rho_i, \quad z_{i-1} < z \leq z_i, \\ z_0 = 0, \quad z_N = z_{max}. \quad (12)$$

The values of the dark energy density ρ_i ($i = 1, 2, \dots, N$) are the independent variables to be estimated from data. Again, we proceed as though we had absolutely no information on the function $\rho_X(z)$, and treat it as a completely arbitrary function.

¹For a complementary method, see [24] which uses a Markov Chain Monte Carlo (MCMC) technique.

It is convenient to trade the $N + 1$ parameters ρ_i with the N parameters f_i and the single parameter Ω_m , where

$$f_i = \frac{\rho_i}{\rho_0} \quad (i = 1, 2, \dots, N) \quad \text{and} \quad \Omega_m = 1 - \frac{\rho_0}{\rho_{\text{crit}}}. \quad (13)$$

We define

$$\rho_0 \equiv \rho_X(0) \quad (14)$$

and take $\rho_{\text{crit}} \equiv 3H_0^2/(8\pi G)$ as the usual critical density. We thus have a total of $N + 2$ parameters: the Hubble constant $h = H_0/(100 \text{ km/s/Mpc})$, the matter energy density parameter Ω_m , and the N parameters f_i ($i = 1, 2, \dots, N$) describing the test dark energy function. The complete set of parameters, then, is

$$\mathbf{s} \equiv (h, \Omega_m, \rho_i), \quad (15)$$

where $i = 1, \dots, N$ as described above. We will vary the number of bins N between 1 and 14, and look for the optimal fit to the data. To illustrate, an arbitrary function may become a good approximation to the data for 4 bins whereas it is a miserable fit for 3 bins.

In [5] we expanded the adaptive iteration method developed in Wang & Garnavich (2001) [11] and Wang & Lovelace (2001) [12] to include arbitrary time dependence of the dark energy density; unlike the earlier papers, we do not restrict ourselves to cases where $\rho'_X(z) \geq 0$.

The adaptive iteration method is designed to optimize the estimation of the dark energy density $\rho_X(z)$ from data. It starts with $f_i = 1$ for all $i = 1, 2, \dots, N$ (a cosmological constant), and builds $f_X(z)$ up iteratively while minimizing a modified $\tilde{\chi}^2$ statistics defined shortly. This adaptive iteration technique is further explained in the Appendix.

We can now determine a best fit to the set of parameters \mathbf{s} by using a χ^2 statistic, with [8]

$$\chi^2(\mathbf{s}) = \sum_l \frac{[\mu_p^{(l)}(z_l|\mathbf{s}) - \mu_0^{(l)}(z_l)]^2}{\sigma_l^2}, \quad (16)$$

where $\mu_p^{(l)}(z_l|\mathbf{s})$ is the prediction for the distance modulus at redshift z_l , given the set of parameters \mathbf{s} , and the sum extends over all the observed SNe Ia. Here σ_l is the dispersion of the measured distance modulus due to intrinsic and observational uncertainties in SN Ia peak luminosity.

Assuming Gaussian errors, the probability density function for the parameters \mathbf{s} is

$$p(\mathbf{s}) \propto \exp\left(-\frac{\chi^2}{2}\right). \quad (17)$$

The normalized probability density function is obtained by dividing the above expression by its sum over all possible values of the parameters \mathbf{s} .

The probability density function of a given parameter s_i is obtained by integrating over all possible values of the other $N + 1$ parameters. To reduce the computation time, we can integrate over the Hubble constant h analytically, and define a modified χ^2 statistic [11] as

$$\tilde{\chi}^2 \equiv \chi_*^2 - \frac{C_1}{C_2} \left(C_1 + \frac{2}{5} \ln 10 \right) - 2 \ln h^*. \quad (18)$$

Here h^* is a fiducial value of the dimensionless Hubble constant h ,

$$\chi_*^2 \equiv \sum_l \frac{1}{\sigma_l^2} \left(\mu_p^{*(l)} - \mu_0^{(l)} \right)^2, \quad (19)$$

$$C_1 \equiv \sum_l \frac{1}{\sigma_l^2} \left(\mu_p^{*(l)} - \mu_0^{(l)} \right), \quad (20)$$

$$C_2 \equiv \sum_l \frac{1}{\sigma_l^2}, \quad (21)$$

with

$$\mu_p^{*(l)} \equiv \mu_p(z_l; h = h^*) = 42.384 - 5 \log h^* + 5 \log [H_0 d_L(z_l)/c], \quad (22)$$

The probability distribution function of the estimated parameters (excluding h) is now $\exp(-\tilde{\chi}^2/2)$. It is straightforward to check that the derivative of $\tilde{\chi}^2$ with respect to h^* is zero; hence our results are independent of the choice of h^* . We take $h^* = 0.65$.

For a given choice of N , we can minimize the modified χ^2 statistic of Eq.(18) to find the best fit Ω_m^{est} and $\rho_X(z)$ (parametrized by ρ_i , $i = 1, 2, \dots, N$).

B. Using the Value of Ω_m to Constrain $\rho'_X(z)$

For the remainder of this Section, we restrict ourselves to Models 1, 2, and 3. We return to Model 4 in the Results Section below.

To reiterate, we have started from three of the models defined in Section III: (1) the cosmological constant model with no time dependence in the energy density, (2) a quintessence model with $\rho'_X(z) \geq 0$, and (3) an MP Cardassian model with $\rho'_X(z) \leq 0$. We have constructed a simulated data set for each of these models, and aim to see how well we can go backwards to determine the sign of $\rho'(z)$ from this fake data set. In other words, can we reconstruct correctly the sign of the time-dependence of the energy density of the true model? To do this, we find (via the adaptive iteration technique) the model that best fits the observed matter density Ω_m .

For a given number of redshift bins N , we can minimize the modified $\tilde{\chi}^2$ statistic of Eq.(18) to find the best fit values Ω_m^{est} and f_i^{est} for Ω_m and $f_X(z) = \rho_X(z)/\rho_X(0)$ parametrized by f_i ($i = 1, 2, \dots, N$). For each model in Table 1, we obtain *three* sets of best fit parameters. We apply three different constraints to the arbitrary function $\rho_X^{test}(z)$ in order to discover which one allows a good fit. The three constraints are:

- (i) $\rho_X^{test}(z) = \rho_X^{test}(0) = \text{constant}$; i.e., a cosmological constant model;
- (ii) $d\rho_X^{test}(z)/dz \geq 0$;
- and (iii) $d\rho_X^{test}(z)/dz \leq 0$.

We note that the second and third test functions are monotonically increasing and decreasing respectively, but do allow portions of the function to be flat as a function of redshift (i.e., constant for some but not all redshifts).

For each of these three constraints, we find the best fit parameters. If our technique works, the trial that gives the Ω_m^{est} closest to the true Ω_m corresponds to the correct underlying theoretical model (Model 1, 2, or 3). For example, for the case where Model 2 ($\rho'_X(z) \geq 0$) is the theoretical model, if the trial with $d\rho_X^{test}(z)/dz \geq 0$ obtains the best value of Ω_m , then we have reproduced the correct time dependence of the dark energy density. Indeed we find that the technique works.

Figure 1 shows our results: panels (a), (b), and (c) correspond to Models 1, 2, and 3. For each of the three models, the figure shows the best fit Ω_m^{est} , under all of the three constraints above, for N values ranging from 1 to 14. The different constraints are represented by different point types. The dot-dashed horizontal line is our fiducial value of $\Omega_m = 0.3$ (i.e., we are assuming that this is the true value of the matter density), and the solid horizontal lines indicate 10% error bars about his fiducial value. We are assuming that Ω_m is known to within 10% from other data sets.

These plots are NOT intended to emphasize the dependence of Ω_m^{obs} on N , the total number of redshifts sampled via linear interpolation (see Eq. (12)). Indeed, as discussed above, the reason that we have found the best fit Ω_m for a variety of N values is simply that the parametrization of the arbitrary function $\rho_X(z)$ may be poor for one value of N but excellent for another. For example, two points ($N = 1$) are perfectly adequate to describe a straight line function, but more points are needed to describe any more complicated function. Any one value of N may (by bad luck) give a bad result. We take a given model to be a good one if it lies within the 10% range on Ω_m for several values of N . The optimal value of N is the one with the lowest $\tilde{\chi}^2$, but we find that $\tilde{\chi}^2$ does not change much over a wide range of possible values of N . We look for stability, i.e. for values of Ω_m^{est} that do not change much as we vary N slightly.

For Model 2 (with $\rho'_X(z) \geq 0$) and Model 3 (with $\rho'_X(z) \leq 0$), as N increases, the estimated values Ω_m^{est} assuming the correct sign of $\rho'_X(z)$ asymptote to the “true” value of $\Omega_m = 0.3$, while the estimated values Ω_m^{est} assuming the wrong sign of $\rho'_X(z)$ asymptote to an incorrect value of Ω_m easily ruled out by observational constraints on Ω_m . Indeed our technique works.

For the cosmological constant model (Model 1, top panel of Fig.1), the estimated Ω_m^{est} values assuming opposite signs for $\rho'_X(z)$ fall roughly symmetrically on opposite sides of the “true” value, and they lie within the error bars on Ω_m . This indicates a degeneracy between Λ models and dark energy models that have mildly time-dependent dark energy density. In other words, it will be difficult to differentiate a constant dark energy density from one that has a very small dependence on redshift. We will examine this possible degeneracy further in Section VI to see how well one can differentiate between these two alternatives.

In conclusion, we can determine the correct sign of $\rho'_X(z)$ if $\rho_X(z)$ is not too close to a constant. To quantify how close to a constant we can go, we need to add error bars to the points in figure 1.

C. Using Monte Carlo to Determine Errors

We evaluate errors by simulating random fluctuations around a fiducial model. A possible choice of fiducial model would be the input (theoretical) model we adopted to generate the SN Ia data set in the first place. However, to be closer to a realistic situation in which

the underlying model has to be determined from data, we will choose our fiducial model to be the model that best fits the data (for us, the simulated data). Specifically, this is the cosmological model with $\rho_X^{\text{BF}}(z)$ (BF = best fit) given by the best-fit values ρ_i^{BF} ($i = 0, 1, \dots, N$) determined above. We have described in the previous section the method by which we obtain our best fit dark energy densities for each of Models 1, 2, and 3. Here, we add random errors to the “measured” distance moduli.

To derive robust error distributions of the estimated parameters Ω_m^{est} and $f_i^{\text{est}} = \rho_i/\rho_0$ ($i = 1, 2, \dots, N$, see Eq.(12)) from each data set, we create 10^3 Monte Carlo samples by adding dispersion in peak luminosity of $\Delta m_{\text{int}} = 0.16$ mag to the distance modulus $\mu_p(z)$ [see Eq.(1)] predicted by the best-fit model (i.e., assuming that the best-fit model is the true model). This is equivalent to making 10^3 new “observations”, each similar to the original data set [21]. The same analysis used to obtain the best-fit model from the data is performed on each Monte Carlo sample. The distributions of the resultant estimates of the parameters (Ω_m^{est} and f_i^{est}) can be used to derive the mean and confidence level intervals of the estimated parameters. Wang & Lovelace [12] showed that such a Monte Carlo analysis gives less biased estimates of parameters than a maximum likelihood analysis, i.e., the Monte Carlo mean of estimated parameters deviate less from the true values of the parameters.

VI. RESULTS

A. Models 1, 2, and 3

Starting from the three dark energy models 1, 2, and 3 in Table 1 with $\rho'_X(z) = 0$, $\rho'_X(z) \geq 0$, and $\rho'_X(z) \leq 0$ respectively, we obtained simulated data sets. Using these simulated data sets², we worked backwards to estimate the best fit values of the $N + 1$ parameters as defined in the previous section. In particular, for each of the simulated data sets we made three trial assumptions, i.e., constant, increasing, and decreasing dark energy density. For each assumption we found an estimate of Ω_m and then ran 1000 Monte Carlo samples to obtain error bars. The results of this analysis are shown in Figure 2. The allowed value of Ω_m , assumed to be known to within 10% is shown with arrows: $\Omega_m = 0.3 \pm 0.03$.

Fig.2 confirms the conclusions that we made based on Fig.1. If the true dark energy density varies with time (quickly enough) and monotonically (see Figs. 2b and 2c), the dark energy models with the wrong sign of $\rho'_X(z)$ or with constant $\rho_X(z)$ are easily ruled out at $\gtrsim 95\%$ C.L. if Ω_m is known to $\sim 10\%$ accuracy. If the true dark energy density is constant with time (Fig. 2a), then while the correct model (Λ model) is favored, the incorrect models (with $\rho_X(z)$ either increasing or decreasing with redshift) could imitate the correct model if the time variation in $\rho_X(z)$ is small enough. We will quantify the size of the degeneracy region shortly (see Fig.5 and related discussion).

²Note that here, once data become available, the “simulated data set” will be replaced by the real data set. We consider three different simulated data sets based on different dark energy models, since the nature of dark energy is unknown.

Note that due to computational constraints, we have chosen $N = 6$ for demonstration. For an actual data set, the Monte Carlo analysis outlined here should be performed for all values of N (from 1 to a reasonably large number).

Figure 3 shows the best fit dark energy density for the simulated data set based on Model 2 (which has $\rho'_X(z) \geq 0$). To obtain figure 3, we take advantage of the fact that our analysis in Fig.2(b) has allowed us to extract the sign of $\rho'_X(z)$, with the assumption that we know Ω_m to 10% accuracy. Once the sign of the time dependence is known, we can deduce the best fit dark energy density $\rho_X(z)/\rho_X(0)$ shown in Fig. 3, estimated from the Monte Carlo analysis of the simulated data set based on Model 2. The solid line is the true model, i.e., the theoretical curve. One can see that the dotted points with error bars, obtained from the simulated data using our technique, match the true model very well. The value of the matter density corresponding to Fig.3 is $\Omega_m = 0.314(0.271, 0.341)$ (mean and 68.3% confidence range). The corresponding figure for Model 3 ($\rho'_X(z) \leq 0$) was published in [5]. Again, one can see that the time dependence of the energy density can be determined quite well.

B. Model 4 (linear equation of state)

Lastly we come to theoretical dark energy models with a linear equation of state $w_X(z) = w_0 + w_1z$. Again, we simulate data based on this underlying model, and again we ask how well we can determine the time dependence of the energy density of each model. This linear form of the equation of state is the most common parametrization used by the community. As stressed previously, one can extract far more information from data if we aim to learn about the properties of the underlying energy density, in this case its time dependence. In fact, because of our ignorance of the true nature of dark energy, it is dangerous to rely on specific parametrizations. Hence, we perform the analysis described in the paper, in which we treat the dark energy density $\rho_X(z)$ as a free function in extracting information from the data (in this case simulated data). We will do a blind test (non-parametric study), in which we do *not* assume the linear form of the equation of state, to see whether the time-variation of dark energy density can be ascertained. This will establish a point of reference with the work by others. In other words, we generate models with a given equation of state but then reconstruct (the time dependence of) the dark energy density itself.

We studied a grid of models, with $-1.2 \leq w_0 \leq -0.5$, and $-1.5 \leq w_1 \leq 0.5$, and a grid spacing of $\Delta w_0 = 0.1$ (0.2 for $w_0 \leq -1$) and $\Delta w_1 = 0.1$. This represents a total of 147 models. For each of these theoretical models, we followed the same procedure described above. First, we simulated data based on each model; next we obtained the best fit $\rho_X^{\text{test}}(z)$ for each model with the adaptive iteration method (the best fit function chosen due to its producing Ω_m^{est} closest to the correct value); finally we created 10^3 Monte Carlo samples (fluctuations about the the best fit function) to obtain error bars. We followed this procedure for each of the 147 models. Fig. 4 shows the estimated Ω_m^{est} values (with 1σ standard deviations) for a subset of the $w_X(z) = w_0 + w_1z$ models that we have studied, assuming: (1) $\rho_X^{\text{test}}(z) = \text{constant}$; (2) $d\rho_X^{\text{test}}(z)/dz \geq 0$ and (3) $d\rho_X^{\text{test}}(z)/dz \leq 0$. The dotted lines in each figure denote $\Omega_m = (0.291, 0.309)$, i.e., assuming that Ω_m is known to 3% from other observations.

Fig. 4 runs through a subset of the grid of theoretical models that we have studied,

namely the models with (a) $w_0 = -1.2$, (b) $w_0 = -1$, and (c) $w_0 = -0.8$. In each plot we have selected one value of w_0 and show results for a variety of values of w_1 . Again, these values of w_0 and w_1 correspond to the underlying theoretical model. Based on each of these sets of w_0, w_1 we simulate data and show how well we can ascertain the time dependence of the dark energy density. We plot the value of Ω_m^{est} with error bars that results from our different trial assumptions, as a function of different (theoretical) values of w_1 in the underlying models. We have obtained three different Ω_m^{est} 's (for the three different trial assumptions) for each underlying w_1 .

In Fig. 4a, we have taken the underlying set of theoretical models to have $w_X(z) = -1.2 + w_1 z$. In other words we took $w_0 = -1.2$ and allowed w_1 to vary from -1.5 to 0.5 with spacing $\Delta w_1 = 0.1$. Our goal is to obtain the correct value of Ω_m^{est} only for the test function that has the correct sign of $\rho'_X(z)$. We see that our technique has indeed reproduced the correct answer, $\rho'_X(z) \leq 0$ for $w_1 < 0$; however, the answer is ambiguous for $w_1 > 0$, where dark energies that are constant or increasing with redshift seem to give equally good fits. In fact we understand the reason for the success of the technique for some values of w_1 and the failure in other regimes, and explain it here. As a reminder, we showed below Eq.(9) that $\rho'_X(z)$ has the same sign as $1 + w_0 + w_1(z)$. Hence, for $w_0 = -1.2$, the sign of $\rho'_X(z)$ is equal to $-0.2 + w_1 z$. As we discussed in the last paragraph of Section III, for $w_0 < 0$ (which is the case for Fig. 4a), the dark energy density is monotonic with redshift for $w_1 < 0$, but nonmonotonic for $w_1 > 0$. However, as our trial functions we have only considered monotonic dark energy densities. Hence it is not surprising that our technique only reproduces the correct time dependence of the dark energy in the regimes of parameter space that correspond to dark energies that are monotonically increasing or decreasing in time. The technique works within the regime of validity of our trial assumptions.

In Fig. 4b, the underlying model is $w_X(z) = -1 + w_1 z$, again for w_1 ranging from -1.5 to 0.5 . In this case the corresponding dark energy density is monotonic with redshift for all values of w_1 , and the technique reproduces the right answer for all w_1 .

In Fig. 4c, the underlying model is $w_X(z) = -0.8 + w_1 z$, again for w_1 ranging from -1.5 to 0.5 . This corresponds to a dark energy density that is monotonic for $w_1 > 0$ but non-monotonic for $w_1 < 0$. The dark energy density grows with redshift until $z_{crit} = (1 + w_0)/|w_1| = 0.2/|w_1|$ (as obtained from Eq.(10)) and then decreases with redshift. However, the value of z_{crit} is so small in most models as to be irrelevant; i.e. the function is essentially monotonically decreasing over most of the redshifts at which supernova data are taken. For example, for $w_1 = -1.5$, $z_{crit} = 0.133$. As w_1 approaches 0, the value of z_{crit} grows; clearly at $w_1 = -0.2$ and $z_{crit} = 1$, the turnover from a growing dark energy density to a decreasing one takes place in the middle redshift of the supernova data. In that case we would expect a constant trial with $\rho'_X(z) = 0$ to be no worse a fit than a monotonically increasing or decreasing one. In other words, a cosmological constant appears to fit the data, although of course it is the wrong answer. Indeed this is borne out by the results of Fig. 4c. Here, our technique is very successful at reproducing the correct sign of the time dependence of the dark energy in those regimes where it is sensible to approximate the dark energy density as being monotonic in time.

Models with $w_0 = -0.9, -0.7, -0.6$, and -0.5 behave similarly to those shown in Fig.4. As w_0 gets less negative, the value of z_{crit} (at which the derivative of the dark energy density changes from positive to negative) gets bigger. Again, our technique works to obtain the

correct time dependence of the dark energy density if it is monotonic in time.

To quantify how much the $\rho'_X(z) \neq 0$ models differ from the Λ models, we have defined a quantity Q as the number of standard deviations in the difference of the average estimated value of Ω_m with constant and non-constant dark energy density,

$$Q \equiv \frac{\left| \langle \Omega_m^{\text{est}} |_{\rho_X = \text{non-const}} \rangle - \langle \Omega_m^{\text{est}} |_{\rho_X = \text{const}} \rangle \right|}{\sqrt{\left(\Delta \Omega_m^{\text{est}} |_{\rho_X = \text{non-const}} \right)^2 + \left(\Delta \Omega_m^{\text{est}} |_{\rho_X = \text{const}} \right)^2}}. \quad (23)$$

The thick solid line in the bottom panel of each section of Fig.4 shows Q as a function of w_1 for various w_0 values. As there are two test functions with time varying dark energy density, $\rho'_X(z) \geq 0$ and $\rho'_X(z) \leq 0$, in the figures we plot the quantity Q for that time varying function that produces the value of Ω_m^{est} that best fits the data.

We note that our work is quite different to prior studies performed by other authors. Previous work (e.g., [9,10,26,27]) has attempted to examine how well one can reconstruct the dark energy equation of state, particularly if one assumes it has the form $w_X(z) = w_0 + w_1 z$. Our study differs from previous studies in being *non-parametric* (hence not dependent on $w_X(z) = w_0 + w_1 z$ being the correct model, but only using it as a test case), and spanning a continuous parameter space in (w_0, w_1) (via smooth interpolations in our grid of 147 models).

How Small Can We Make the Region of Degeneracy?

We can ask the question: what is the range of (w_0, w_1) over which one cannot determine the sign of the time dependence? In other words, what is the range of degeneracy between a cosmological constant and a time-changing vacuum energy appearing to fit the data equally well? And how far can it be shrunk down?

Fig.5 shows the (w_0, w_1) parameter space that we have studied. The models that lie within the shaded region cannot be differentiated from a Λ model even if Ω_m is known to 1%. Similarly, models which lie within the dotted, dashed, and solid lines cannot be differentiated from a cosmological constant model if Ω_m is known to within 3%, 5%, and 10% accuracies respectively.

The degeneracy region shown in Fig.5 is centered about the line

$$1 + w_0 \simeq -\frac{z_{\text{max}}}{3} w_1, \quad (24)$$

where z_{max} is the maximum redshift of the survey ($z_{\text{max}} = 1.7$ for SNAP).

In the parameter space outside of the shaded region in Fig.5, $\rho'_X(z) \neq 0$ models are preferred over the Λ models if Ω_m is known to 1% accuracy, indicating our ability to detect the time-variation of the dark energy density at 1σ or higher significance levels.

Finally, we point out a way to reduce the degeneracy by taking advantage of the fact that the slope in Eq.(24) changes for different values of z_{max} . Hence changing z_{max} will rotate the degeneracy region in (w_0, w_1) . One can choose a variety of different values of z_{max} to break the degeneracy. In other words, in addition to using the entire data set, one can restrict the data out to a variety of different cutoff redshifts to obtain complementary information. If, in addition to the full data set, we consider only those data to a second maximum redshift $z_{2,\text{max}}$, we can reduce the degeneracy region in Fig.5 significantly. In

Figure 5 we have plotted both the degeneracy region obtained using all the data, as well as dot-dashed lines illustrating the different degeneracy region if only data out to $z_{2,max} = 0.5$ were used.³ The combination of information from these dot-dashed lines together with the shaded region allow us to break the degeneracy substantially. The shaded region in Fig.5 bounded by dot-dashed lines illustrates the smallest possible degeneracy region if Ω_m is known to 1%.

VII. CONCLUSIONS

We have investigated how well future supernova data from dedicated telescopes (such as SNAP), when combined with data of nearby supernovae, can be used to determine the time dependence of the dark energy density. For quantitative comparison, we have done an extensive study of a number of dark energy models, with dark energy density that is constant, increasing, and decreasing in time. Based on these models we have simulated data sets in order to show that we can indeed reconstruct the correct sign of the time dependence of the dark energy density.

Among the dark energy models we studied are those parametrized by an equation of state $w_X(z) = w_0 + w_1 z$. Here, $w \equiv p/\rho$. We studied a grid of 147 models, for $-1.2 \leq w_0 \leq -0.5$, and $-1.5 \leq w_1 \leq 0.5$. We emphasize that it is the dark energy density that we reconstructed, *not* the equation of state. We find that there is a degeneracy region in the (w_0, w_1) parameter space centered near $1 + w_0 = -w_1 z_{max}/3$ (where z_{max} is the maximum redshift of the survey, e.g., $z_{max} = 1.7$ for SNAP); the models that lie within this region cannot be differentiated from a Λ model even if Ω_m is known independently to 1% accuracy (we compute the size of the region for Ω_m known to varying degrees of accuracy). Outside of this degeneracy region, we can detect the time variation of the dark energy density at 1σ or higher significance levels.

We emphasize that, given the same data, one can learn much more by reconstructing the dark energy density directly (and its time dependence) than by attempting to reconstruct its equation of state.

ACKNOWLEDGMENTS

It is a pleasure for us to thank Greg Tarle for helpful comments. We acknowledge support from NSF CAREER grant AST-0094335 (Y.W. and V.K.); the Department of Energy grant at the University of Michigan and the Michigan Center for Theoretical Physics (K.F.); the DOE at Fermilab and Chicago, from NASA grant NAG5-10842 at Fermilab, and from the NSF Center for Cosmological Physics at Chicago (J.A.F).

APPENDIX: ADAPTIVE ITERATION TECHNIQUE

³These are qualitative illustrations, not from actual calculations (which would involve lengthy computations).

The goal of the adaptive iteration technique is to reconstruct (as accurately as possible) the function $f_X(z) = \rho_X(z)/\rho_X(0)$ from a simulated data set. We start from a time independent function (in which $f_X(z) = 1$ for all z) and build up the function iteratively to find that function which best matches the data.

To illustrate the adaptive iteration technique, we present an example. In this appendix we here restrict our discussion to monotonically increasing forms of $f_X(z)$. Let us consider the case where we break up the function (and the simulated data) into five equally spaced bins in redshift space, i.e., $N = 5$ so that z ranges from 0, z_1, z_2, z_3, z_4, z_5 . We will start with a flat function, $f_X(z) = \rho_X(z)/\rho_X(0) = 1$ and build up from there. In all the iterations, we will always keep $f_X(0) = \rho_X(z = 0)/\rho_X(0) = 1$ fixed (it's an identity equation since $\rho_X(0) \equiv \rho_X(z = 0)$), and vary $f_X(z)$ at the other values of z . Here is how we proceed in the first iteration:

- (1) Compute χ^2 for $f_X(z) = 1$.
- (2) Increase $f_X(z_i)$ for all $i = 1, 2, 3, 4, 5$ by one stepsize, Δ , i.e., $f_X(z_i) = 1 + \Delta$ for all $i = 1, 2, 3, 4, 5$. Compute χ^2 . If the current χ^2 is smaller than the previous χ^2 (from the previous step), the new $f_X(z_i)$ values are favored; keep them. Otherwise, the previous values of $f_X(z_i) = 1$ are favored. As stepsize we used primarily $\Delta = 0.01$, but also $\Delta = 0.05$ and 0.1 for comparison. We find that the results are not sensitive to the stepsize; of course, the smaller the stepsize, the longer the running time.
- (3) Increase $f_X(z_i)$, $i = 2, 3, 4, 5$ by one stepsize, Δ , i.e., $f_X(z_i) = f_X(z_i)^{prev} + \Delta$, $i = 2, 3, 4, 5$, where $f_X(z_i)^{prev}$ are the $f_X(z_i)$ values favored by the previous step. Compute χ^2 . If the current χ^2 is smaller than the previous χ_{min}^2 (from the previous step), the new $f_X(z_i)$ values are favored; keep them. Otherwise, $f_X(z_i)^{prev}$ are favored.
- (4) Increase $f_X(z_i)$, $i = 3, 4, 5$ by one stepsize, Δ , i.e., $f_X(z_i) = f_X(z_i)^{prev} + \Delta$, $i = 3, 4, 5$, where $f_X(z_i)^{prev}$ are the $f_X(z_i)$ values favored by the previous step. Compute χ^2 . If the current χ^2 is smaller than the previous χ_{min}^2 (from the previous step), the new $f_X(z_i)$ values are favored; keep them. Otherwise, $f_X(z_i)^{prev}$ are favored.
- (5) Increase $f_X(z_i)$, $i = 4, 5$ by one stepsize, Δ , i.e., $f_X(z_i) = f_X(z_i)^{prev} + \Delta$, $i = 4, 5$, where $f_X(z_i)^{prev}$ are the $f_X(z_i)$ values favored by the previous step. Compute χ^2 . If the current χ^2 is smaller than the previous χ_{min}^2 (from the previous step), the new $f_X(z_i)$ values are favored; keep them. Otherwise, $f_X(z_i)^{prev}$ are favored.
- (6) Increase $f_X(z_i)$, $i = 5$ by one stepsize, Δ , i.e., $f_X(z_i) = f_X(z_i)^{prev} + \Delta$, $i = 5$, where $f_X(z_i)^{prev}$ are the $f_X(z_i)$ values favored by the previous step. Compute χ^2 . If the current χ^2 is smaller than the previous χ_{min}^2 (from the previous step), the new $f_X(z_i)$ values are favored; keep them. Otherwise, $f_X(z_i)^{prev}$ are favored.

In the second iteration, repeat steps (2)-(6), but with these changes in step 2: replace $f_X(z_i) = 1 + \Delta$ with $f_X(z_i) = f_X(z_i)^{prev} + \Delta$, replace “the previous χ^2 ” with “the previous χ_{min}^2 ”, and replace “the previous values of $f_X(z_i) = 1$ ” with “ $f_X(z_i)^{prev}$ ”.

Subsequent iterations follow the same procedure as the second iteration. Continue the iterations until χ_{min}^2 stops changing.

We successively perform further iterations to ascertain the function $\rho_X(z)$ that best fits the data. As described here, one can only end up with a monotonically increasing form for $\rho(z)$. For monotonically decreasing function, the procedure is exactly the same, with $+\Delta$ replaced by $-\Delta$.

REFERENCES

- [1] C. Bennett, et al. (the WMAP team), astro-ph/0302208; D. Spergel, et al. (the WMAP team), *Astrophys.J.Suppl.* **148**, 175 (2003).
- [2] K. Freese, F.C. Adams, J.A. Frieman, & E. Mottola, *Nucl. Phys.* **B287**, 797 (1987); P.J.E. Peebles & B. Ratra, *ApJ* **325L**, 17 (1988); C. Wetterich, *Nucl. Phys.* **B302**, 668 (1988); J. Frieman, C. Hill, A. Stebbins, and I. Waga, *Phys.Rev.Lett.* **75**, 2077 (1995), I. Zlatev, L. Wang, and P.J. Steinhardt, *Phys. Rev. Lett.* **82**, 896 (1999).
- [3] K. Freese, and M. Lewis, *Phys.Lett.* **B540**, 1 (2002); K. Freese, *Nuclear Physics B (Proc. Suppl.)* **124**, 50 (2003)
- [4] P. Gondolo and K. Freese, *Phys.Rev.* **D68** 063509 (2003)
- [5] Y. Wang, K. Freese, P. Gondolo, and M. Lewis, *Astrophys.J.* **594**, 25 (2003).
- [6] L. Parker and A. Raval, *Phys. Rev. D* **60**, 063512 (1999); C. Deffayet, *Phys. Lett.* **B502**, 199 (2001); N. Bilic, G.B Tupper, and R. Viollier, *Phys.Lett.* **B535** 17 (2002); M. Ahmed, S. Dodelson, P.B. Greene, and R. Sorkin, astro-ph/0209227; S. Capozziello, S. Carloni, and A. Troisi, astro-ph/0303041; S. Carroll, V. Duvvuri, M. Trodden, and M. Turner, astro-ph/0306438.
- [7] A. G. Riess, *et al.* [Supernova Search Team Collaboration], *Astron. J.* **116**, 1009 (1998) [arXiv:astro-ph/9805201].
- [8] S. Perlmutter, *et al.* [Supernova Cosmology Project Collaboration], *Astrophys. J.* **517**, 565 (1999) [arXiv:astro-ph/9812133].
- [9] I. Maor, R. Brustein, and P.J. Steinhardt, *Phys. Rev. Lett.* **86**, 6 (2001); I. Maor, R. Brustein, J. McMahon, and P.J. Steinhardt, *Phys. Rev. D* **65**, 123003 (2002).
- [10] V. Barger and D. Marfatia, *Phys. Lett.* **B498**, 67 (2001).
- [11] Y. Wang, and P. Garnavich, *ApJ*, 552, 445 (2001)
- [12] Y. Wang, and G. Lovelace, *ApJ*, 562, L115 (2001)
- [13] M. Tegmark, *Phys. Rev. D* **66**, 103507 (2002)
- [14] R.A. Daly, S.G. & Djorgovski *ApJ*, 597, 9 (2003)
- [15] M.M. Phillips, *ApJ*, 413, L105 (1993)
- [16] A.G. Riess, W.H. Press, and R.P. Kirshner, *ApJ*, 438, L17 (1995)
- [17] C.B. Netterfield *et al*, *Ap. J.* **571**, 604 (2002); R. Stompor *et al*, *Ap. J. Lett.* **561**, 7 (2001); N.W. Halverson *et al*, *Ap. J.* **568**, 38 (2002).
- [18] S. Weinberg, "Gravitation and Cosmology" (John Wiley & Sons, New York, 1972)
- [19] P. Schueker, *et al*, *Astron. Astrophys.*, **402**, 53 (2003)
- [20] A. Melchiorri, L. Mersini, C.J. Odman, and M. Trodden, *Phys.Rev.* **D68** 043509 (2003)
- [21] W. H. Press, S. A. Teukolsky, W. T. Vetterling, B.P. Flannery, "Numerical Recipes in Fortran 77 (The Art of Scientific Computing)" (Cambridge University Press, 2nd ed., 1992)
- [22] Y. Wang, *ApJ*, 531, 676 (2000a)
- [23] Y. Wang, *ApJ*, 536, 531 (2000b)
- [24] Y. Wang, P. Mukherjee, astro-ph/0312192, *ApJ* in press (2004)
- [25] G. Tarle, (for the SNAP Collaboration), astro-ph/0210041
- [26] D. Huterer and M.S. Turner, *Phys.Rev.* **D64** 123527 (2001)
- [27] E.V. Linder and D. Huterer, *Phys. Rev. D* **67**, 081303 (2003)

FIGURES

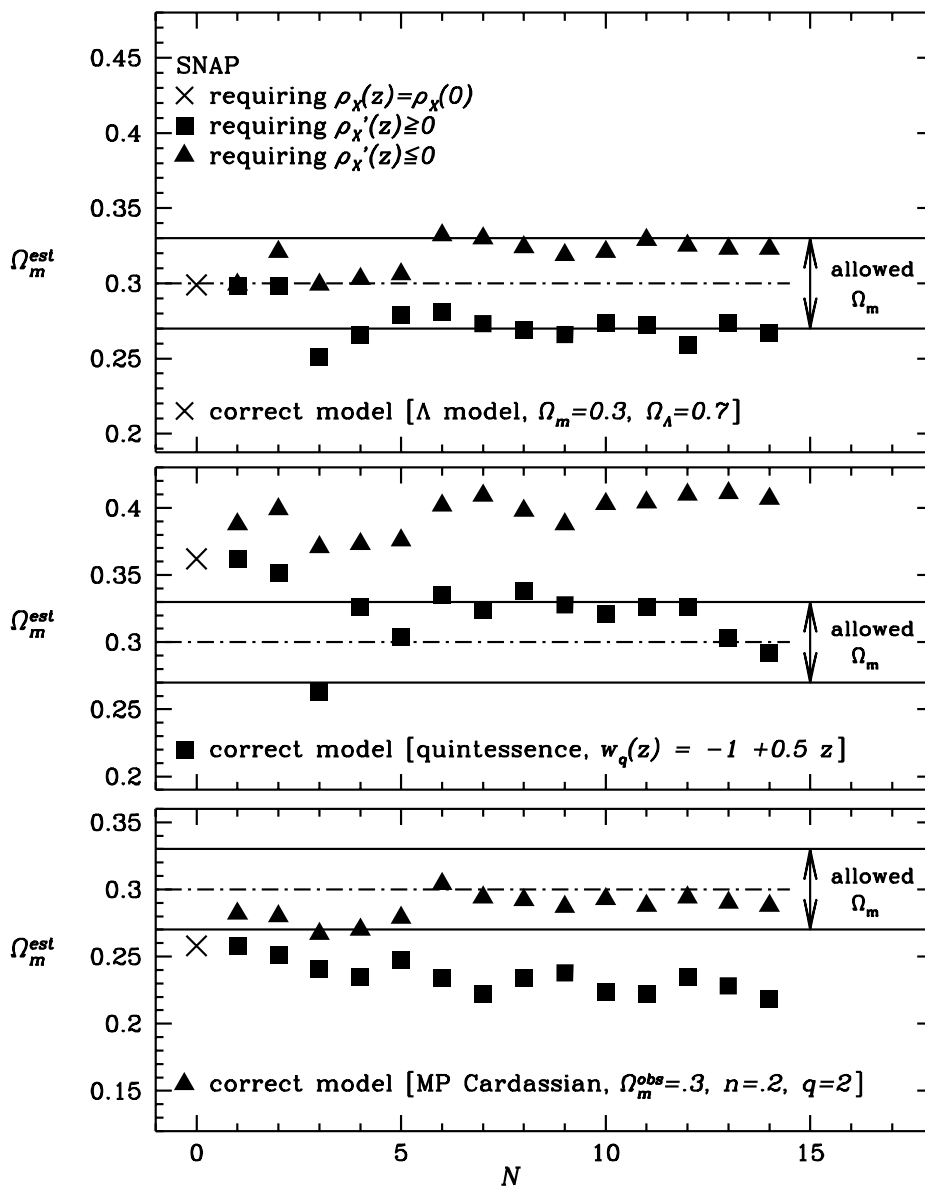


FIG. 1. The estimated best fit Ω_m^{est} , shown for a variety of values of the number of parameters N . The three panels are for the dark energy models 1, 2, and 3 (given in Table 1) respectively. Each panel plots the estimated Ω_m^{est} for three trial functions: crosses indicate constant $\rho_X^{test}(z)$, squares indicate $d\rho_X^{test}/dz > 0$, and triangles indicate $d\rho_X^{test}/dz < 0$. The dot-dashed line indicates the “true” value of $\Omega_m = 0.3$ in each model, the solid lines indicate the $\pm 10\%$ range of Ω_m . In each panel the test function with the correct time dependence (same as the underlying theoretical model) produces an acceptable Ω_m^{est} that matches data; the test function with the wrong time dependence produces an incorrect value of Ω_m and hence can be ruled out. This technique can reproduce the correct time dependence of the dark energy density.

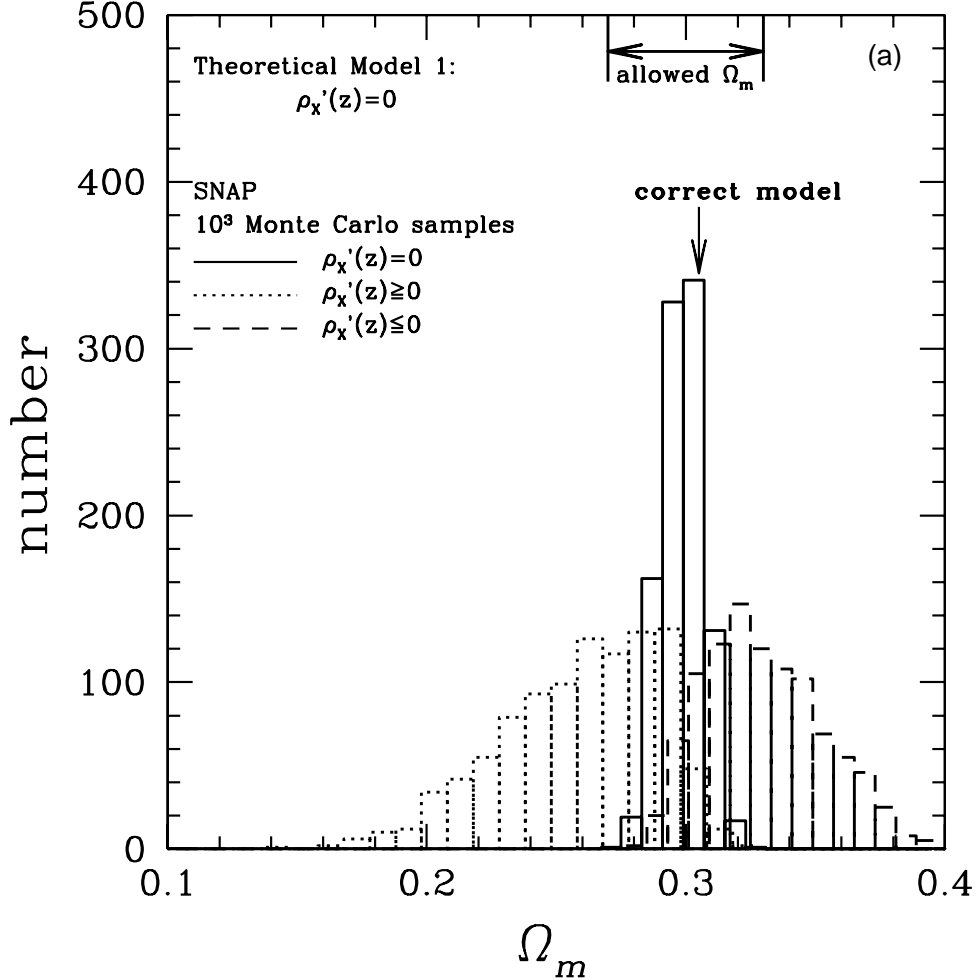


FIG. 2. (a) Distributions of the estimated Ω_m values from 10^3 Monte Carlo samples. Here, the underlying theoretical model is a cosmological constant. The Monte Carlo samples are obtained under three different trial assumptions about the time dependence of the dark energy $\rho'_X(z)$: increasing, decreasing, or constant. The allowed value of $\Omega_m = 0.3 \pm 0.03$ is indicated. The correct value of Ω_m is reproduced for the correct time dependence of the dark energy, $\rho'_X = 0$; hence one is led to conclude that the underlying model is a cosmological constant. Note, however, that for this case some of the models with time dependent ρ_X also produce the right values of Ω_m , so that there is some degeneracy.

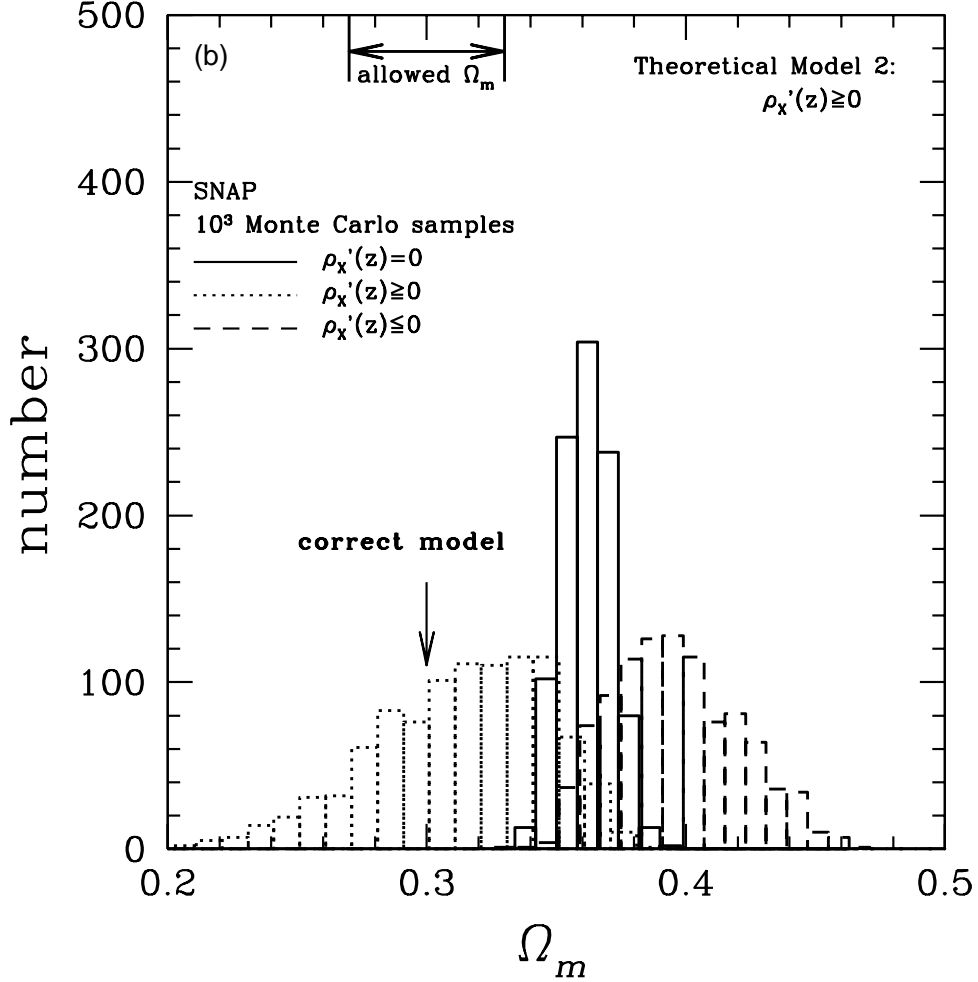


FIG. 2. b) Same as Fig.2(a), but for the simulated data set based on Model 2. Upon running 10^3 Monte Carlo samples, the correct value of Ω_m is reproduced only for the trial functions with $\rho'_X > 0$, which agrees with the time dependence of the underlying model. [The underlying model is a quintessence model with $w_x(z) = -1 + 0.5z$ and $\rho'_X(z) > 0$.] We have taken $N = 6$ for illustration. Hence one recovers the correct time dependence of the energy density.

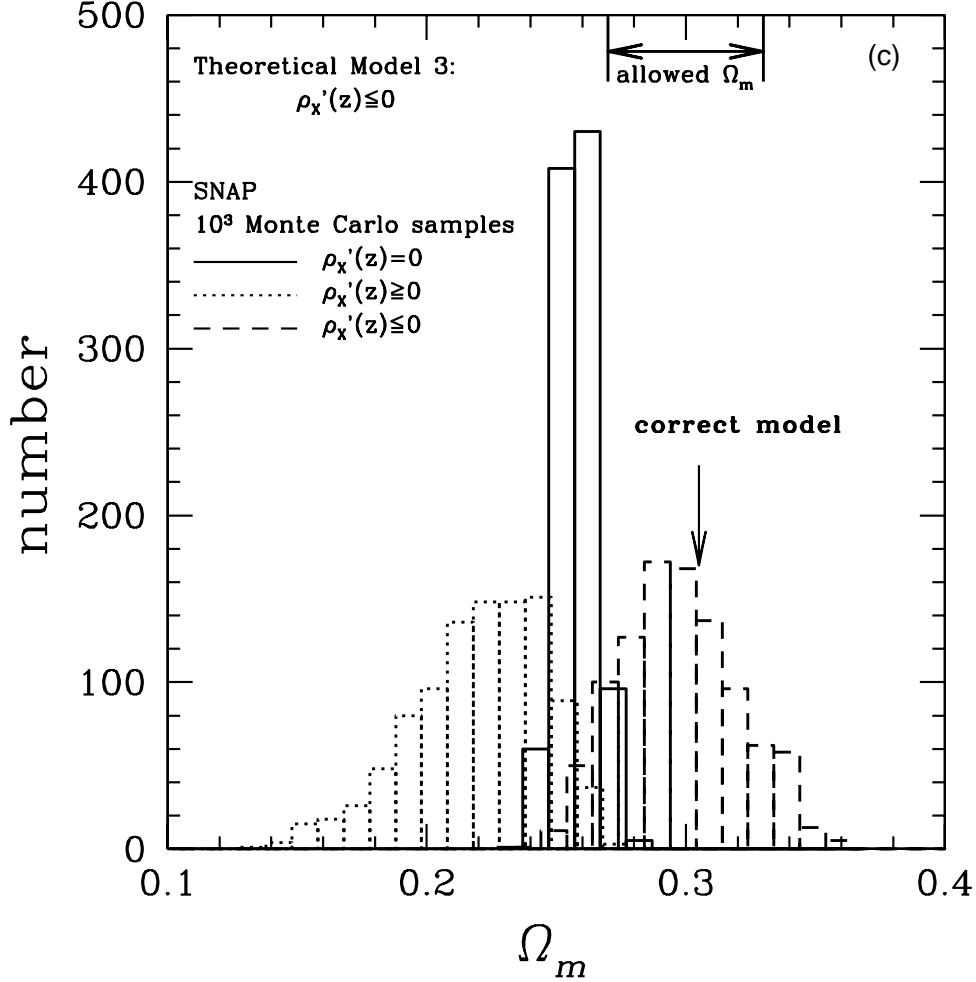


FIG. 2. c) Same as Fig.2(a), but for the simulated data set based on Model 3. Upon running 10^3 Monte Carlo samples, the correct value of Ω_m is reproduced only for the trial functions with $\rho'_X < 0$, which agrees with the time dependence of the underlying model. [The underlying model is a MP Cardassian model with $n=0.2$ and $q=2$, and $\rho'_X(z) < 0$.] We have taken $N = 6$. Hence one again recovers the correct time dependence of the energy density.

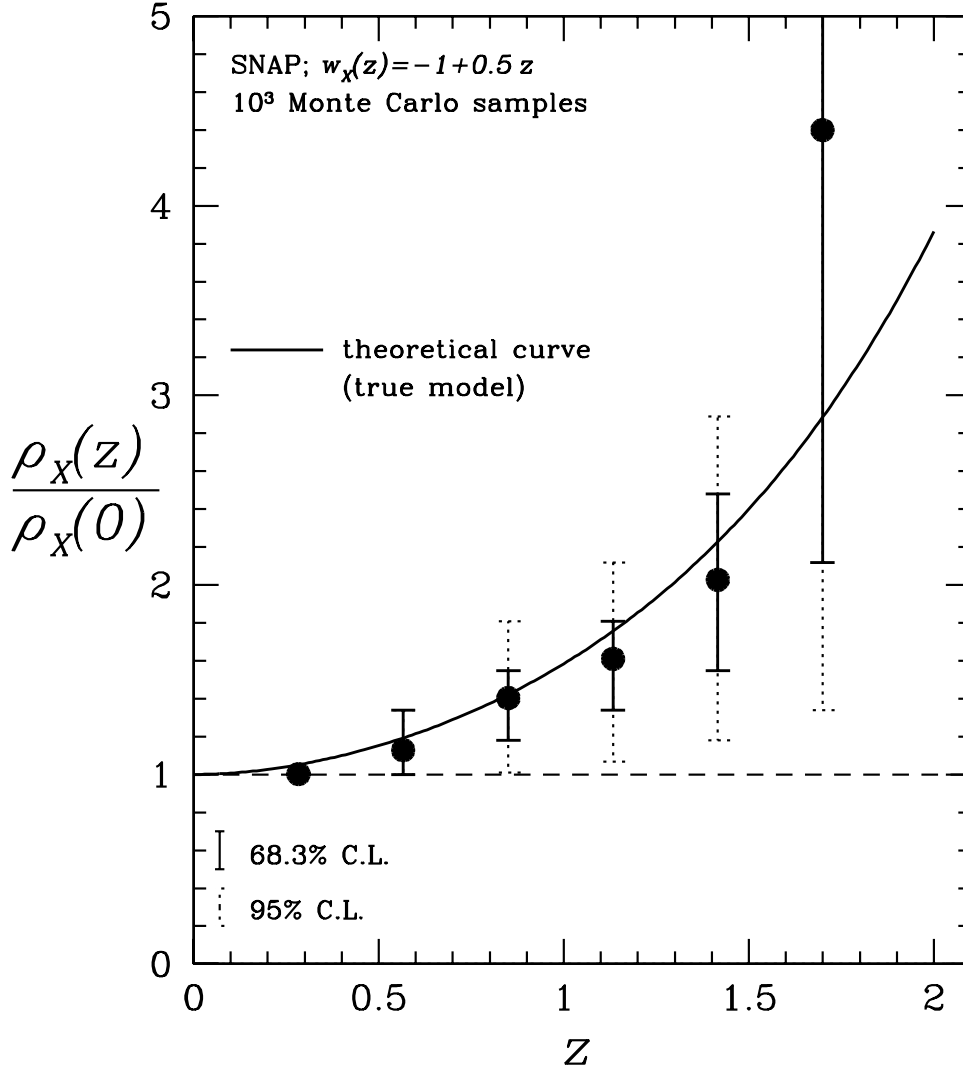


FIG. 3. Best fit dark energy density $\rho_X(z)/\rho_X(0)$ estimated from the Monte Carlo analysis of the simulated data set based on Model 2, which has $\rho'_X(z) > 0$. This plot assumes that Ω_m is known to 10% accuracy [and that the sign of the time dependence has been extracted as shown in Figure 2]. The solid line is the true model, i.e., the theoretical curve. One can see that the dotted points with error bars, obtained from the simulated data using our technique, match the true model very well. Here, we have taken $N = 6$.

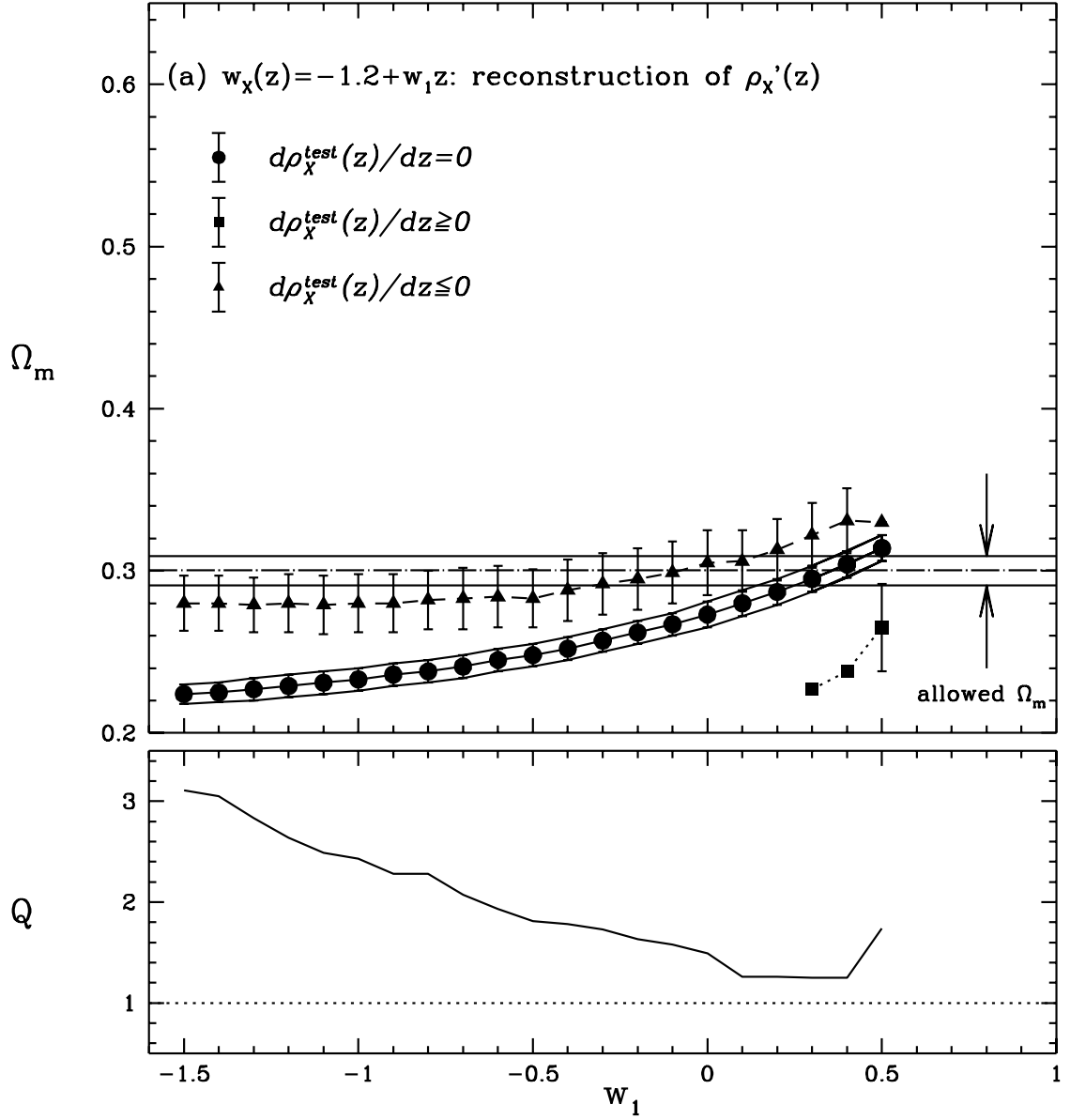


FIG. 4. The estimated Ω_m values (with 1σ standard deviations) for $w_X(z) = w_0 + w_1z$ models. In each plot in panels a-g, we have selected one value of w_0 and show results for a variety of values of w_1 ; these values of w_0 and w_1 correspond to the underlying theoretical model. Based on each of these sets of w_0, w_1 we simulated data, and in the upper half of each panel, plotted the values of Ω_m^{est} with error bars that result from our three different trial assumptions, as a function of different (theoretical) values of w_1 in the underlying models. The three different trial assumptions are represented by: circles for $\rho_X^{test} = \text{constant}$, squares for $d\rho_X^{test}/dz \geq 0$, and triangles for $d\rho_X^{test}/dz \leq 0$. The dotted lines denote $\Omega_m = (0.291, 0.309)$ (here, we assume that Ω_m is known to 3% from other observations.) In the lower half of each panel, we have plotted the quantity Q defined in Eq.(23), the number of standard deviations in the difference of the average estimated value of Ω_m with constant and non-constant dark energy density.

(a) Underlying theory: $w_0 = -1.2$ and $-1.5 \leq w_1 \leq 0.5$. The correct value of Ω_m is obtained for $\rho'_X(z) \leq 0$ for $w_1 < 0$; here our technique has indeed reproduced the correct time dependence of the dark energy. However, the answer is ambiguous for $w_1 > 0$, where the underlying theory is non-monotonic.

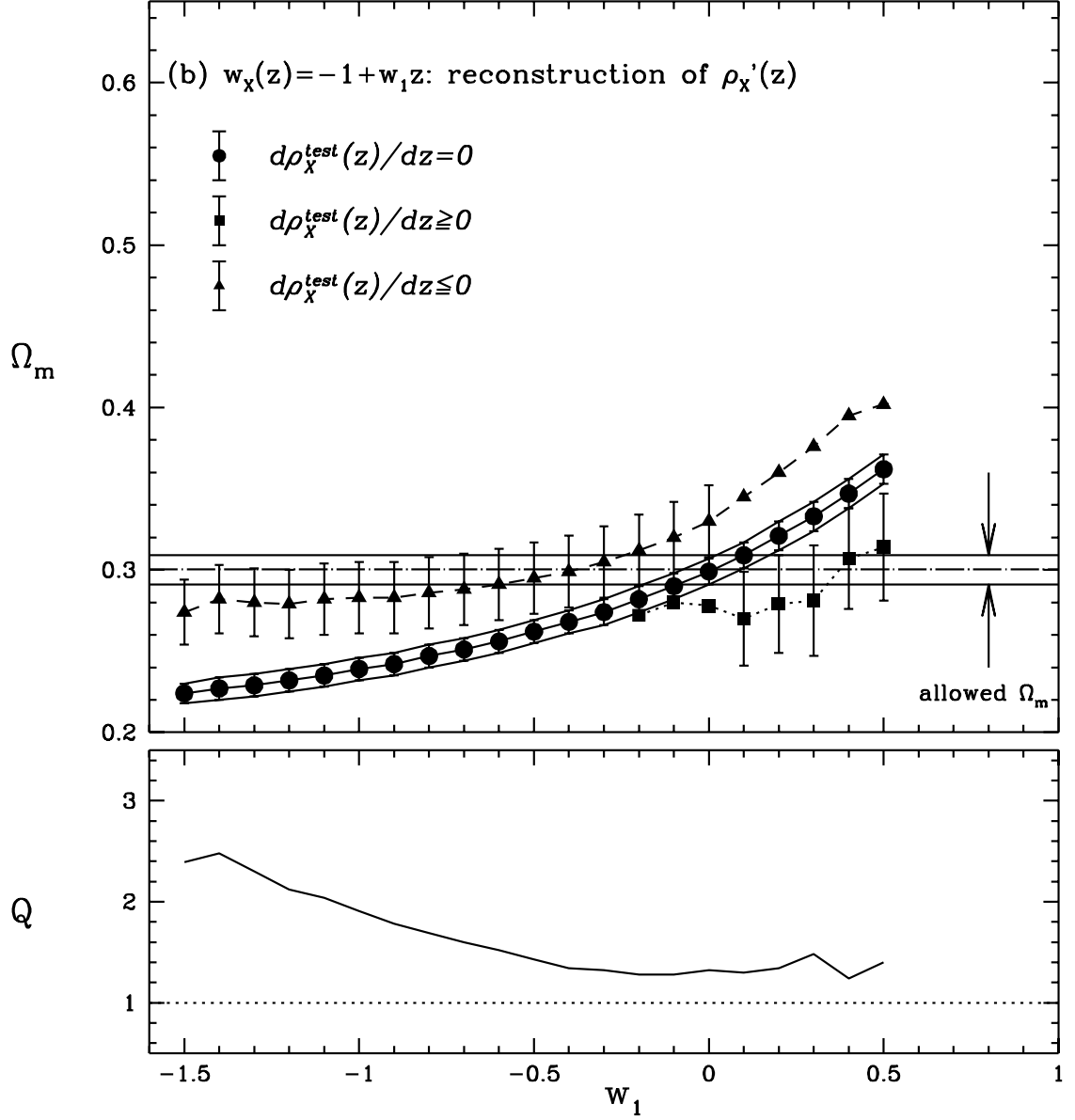


FIG. 4. (b) Underlying theory: $w_0 = -1$ and $-1.5 \leq w_1 \leq 0.5$. Here our technique obtains an allowed value of Ω_m and hence reproduces the correct time dependence of the dark energy for all w_1 .

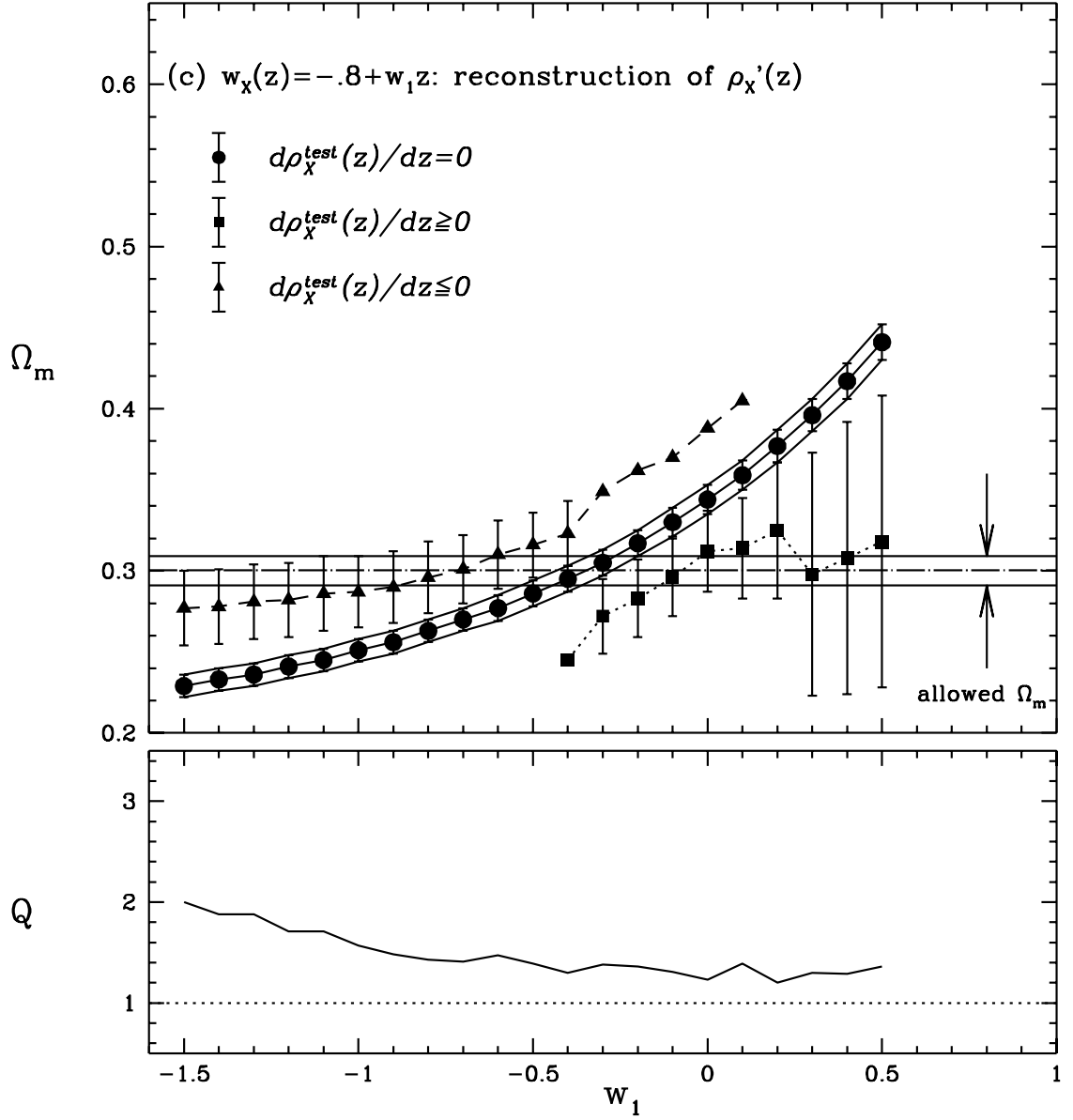


FIG. 4. (c) Underlying theoretical model: $w_0 = -0.8$ and $-1.5 \leq w_1 \leq 0.5$ (see discussion in text).

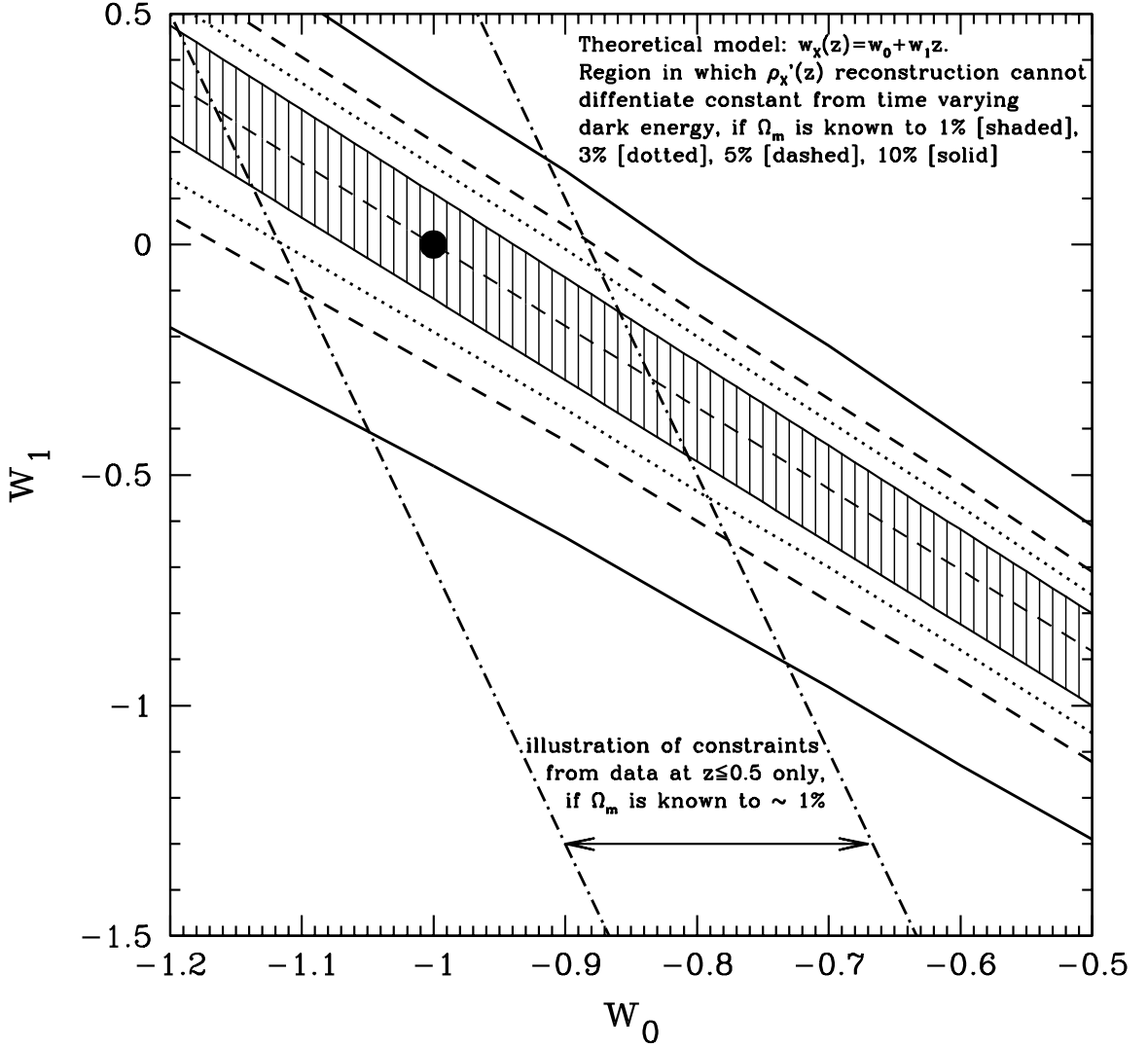


FIG. 5. The (w_0, w_1) parameter space that we have studied. For the theoretical models with w_0 and w_1 that lie within the shaded region, the reconstructed $\rho'_X(z)$ cannot be differentiated from a Λ model (indicated by a fat circle) even if Ω_m is known to 1%. Outside of this region, the sign of $\rho'_X(z)$ can clearly be ascertained (if Ω_m is known to 1%). Similarly, models which lie within the dotted, dashed, and solid lines cannot be differentiated from a constant $\rho'_X(z) = 0$ model if Ω_m is known to within 3%, 5%, and 10% accuracies respectively. The degeneracy region is centered about the line $1 + w_0 \simeq -\frac{z_{max}}{3} w_1$, where z_{max} is the maximum redshift of the survey ($z_{max} = 1.7$ for SNAP). The dot-dashed line illustrates (roughly) the different degeneracy region if only those data out to a cutoff redshift of 0.5 were used, if Ω_m were known to 1%. Note that the degeneracy can be reduced by examining different portions of the data out to different redshifts.